Study of Electrical and Optical Properties of Iron Doped Zinc Oxide Thin Films Grown by Spin Coating Method for Optoelectronic Devices

By

Samuel Belayneh

A Thesis Submitted to the Department of Applied Physics

School of Applied Natural Science (SoANS)

Presented in Partial Fulfillment of the Requirement for the Master's Degree in Applied Physics (Material Physics)

Office of Graduate Studies
Adama Science and Technology University

Adama

July, 2021

Study of Electrical and Optical Properties of Iron Doped Zinc Oxide Thin Films Grown by Spin Coating Method for Optoelectronic Devices

By

Samuel Belayneh

Advisor

Megersa Wodajo (PhD)

A Thesis Submitted to the Department of Applied Physics

School of Applied Natural Science (SoANS)

Presented in Partial Fulfillment of the Requirement for the Master's Degree in Applied Physics (Material Physics)

Office of Graduate Studies
Adama Science and Technology University

Adama

July, 2021

Approval of Board of Examiners

We, the undersigned, members of the Board of Examiners of the final open defense by Samuel Belayneh have read and evaluated his thesis entitled “Study of Electrical and Optical Properties of Iron Doped Zinc Oxide Thin Films Grown by Spin coating method for Optoelectronic Devices” and examined the candidate. This is, therefore, to certify that the thesis has been accepted in partial fulfillment of the requirement of the Degree of Master’s.

Name	Signature	Date
_____ (Advisor)	_____	_____
_____ (Chairperson)	_____	_____
_____ (Internal Examiner)	_____	_____
_____ (External Examiner)	_____	_____

Advisor's Approval Sheet

To: Applied Physics Department

Subject: Thesis Submission

This is to certify that the thesis entitled "Study of Electrical and Optical Properties of Iron Doped Zinc Oxide Thin Films Grown by Spin coating method for Optoelectronic Devices" submitted in partial fulfillment of the requirements for the degree of Master's in Material Physics, the Graduate program of the department of Applied Physics, has been carried out by Samuel Belayneh, Id. No R/19500/12, under my supervision. Therefore, I recommend that the student has fulfilled the requirements and hence hereby he can submit the thesis to the department.

Name of Advisor	Signature	Date

Declaration

I hereby declare that this MSc thesis is my original work and has not been presented for a degree in any other university, and all sources of material used for this thesis have been duly acknowledged.

Name: Samuel Belayneh

Signature: _____

This MSc thesis has been submitted for examination with my approval as thesis advisor.

Name: Megersa Wodajo (PhD)

Signature: _____

Date of Submission: July 14, 2021

ACKNOWLEDGEMENT

First of all I would like to express my gratitude to my advisor Dr. Megersa Wodajo for the valuable help he has provided me. He gave me important resources that I can use toward the preparation of this thesis. I would also like to thank Mr. Alemayehu Girma, Mr. Wegene Lema, Mr. Eninges Asmare and other AAU stuffs for their nonstop and unconditional help that has enabled me to carry out and finish my research. My deep gratitude also goes to Adama Science and Technology University for giving me this scholarship to study and achieve my goals.

Table of Contents

List of Figures

List of Acronyms

TM: transition metal,

CBD: chemical bath deposition,

SEM: scanning electron microscope,

DMS: dilute magnetic semiconductor,

XRD: X-ray diffraction,

XRC: x-ray crystallography,

PL: photoluminescence,

LED: light emitting diodes,

UV-Vis: ultraviolet-visible,

RPM: rotation per minute.

List of Tables

Abstract

In this study the effect of iron doping on zinc oxide nanoparticles was investigated for optoelectronic application. Zinc oxide thin films were grown on microscopic glass slides using spin coater by varying the iron concentration by 1%, 3%, 5% and 10% and calcinating all the samples at 500 ^{0}c for 2 hours. The XRD analysis showed the formation of polycrystalline zinc oxide thin films with hexagonal wurtzite structure. The lattice constants and grain size were observed to decrease while the lattice defects increased up on increasing the iron concentration. Optical analysis done using UV-Vis and photoluminescence spectroscopy revealed enhanced visible light absoption and emission behavior of the doped ZnO thin films compared to the undoped ZnO thin film. The energy band gap also decreased from 3.29 eV for the undoped thin film to 3.25 eV for 3% iron doped thin film. Increased iron concentration beyond 3% was observed to impart blue light absorption ability to the thin films due to increased effect of deep levels of the oxygen vacancies. The emission spectra of the samples were observed to red shift revealing non-radiative energy loses due to lattice vibration. The Hall measurement results indicated that all films had good electron conductivity and mobility which make them useful for optoelectronic devices. Considering the results from all measurement, the thin film with 3% iron was found to be optimal for optoelectronic application due to its relatively lower defects, visible light absorption as well as good electron conductivity and mobility.

1. Introduction

1.1 Background of the Study

Zinc oxide, a well-known piezoelectric and electro-optic material with wide direct band gap (3.37 eV) and large exciton binding energy (60 meV) (Srikant & Clarke, 1998), is now being considered as a potential material for a wide range of applications such as optoelectronic and luminescent devices as well as chemical sensors. Extensive studies have been carried out to modify the properties of ZnO for different applications (Muslih & Munir, 2004). For example, a variety of elements have been proposed to be incorporated in to ZnO intentionally to manipulate the optical and electrical properties of the ZnO host. The band gap of ZnO could be increased or reduced by doping with Mg or Cd (Kaphle *et al*., 2004), respectively. Transparent conductive ZnO films with low resistivity as well as high visible transmittance could be realized by doping with the elements Al, Ga and In (Pradeev *et al*., 2007).

The transition metal (TM) doped ZnO has been identified as a promising one, because the host material, ZnO, is a chemically and thermally stable n-type II–VI compound semiconductor with a wide band gap energy (3.37 eV) and a large exciton binding energy (60 meV). During the past years, transition metals have been doped into the ZnO lattice to modulate the local electronic structure and cause dramatic changes in their optical and electromagnetic properties. Until recently, most studies have been focused on the fabrication of Co- or Mn-doped ZnO systems as well as modification of their structural, optical and magnetic properties (Magar *et al*., 2009). However, relatively little attention has been paid to Fe-doped ZnO films.

So far, ZnO-based thin films have been prepared by many different techniques based on vacuum deposition and solution-based processes. While physical methods are capable of producing high-quality and single-crystalline nanostructures, these processes run into some deterrents notably high temperature synthesis, ultra-high vacuum in some cases, and other restrictions in terms of sample uniformity, substrate choice, and low product yield (Kripal *et al*., 2011). On the contrary, the chemical processes do not undergo these drawbacks and are capable of producing unconventional shapes and structures. A wide variety of chemical methods have been reported in the literature such

as chemical bath deposition (CBD), electro-deposition, hydrothermal, spray pyrolysis, spin coating, ultrasonic spray pyrolysis and co-precipitation method.

Several works have been done on modifying some important properties of zinc oxide semiconductor. Cheng and Ma (2009) synthesized a series of $Zn_{1-x}Fe_xO$ thin films with the atomic fraction, x, in the range of 0.011–0.20 on Al_2O_3 substrates at 400^oC by magnetron co-sputtering technique. They performed systematic study on structural, optical and magnetic properties of the film as a function of Fe concentration. The XRD analysis showed that only single ZnO wurtzite phase with (002) preferential orientation was observed, suggesting that the Fe-doped ZnO thin films retained the same crystalline structure and high c-axis orientation as the undoped ZnO films (Cheng & Ma, 2009). With increasing Fe concentration, x, in the films the clear shifts of the (002) peaks to higher angles were observed. This phenomenon indicates a reduction in the lattice constant with Fe doping, which is expected as smaller Fe ions are incorporated into the Zn sites of the ZnO lattice without changing the wurtzite structure.

According to Pearton *et al.* (2007), the UV-visible characterization of iron doped zinc oxide, synthesized through sol-gel method, showed that as Fe concentration was increased, the optical band gap shifted slightly to lower energies than that of the pure ZnO films and also the peak intensity of the UV emission increased, whereas the visible emission intensity decreased. They also found that doping zinc oxide with iron resulted in ferromagnetism in the semiconductor which increased with increasing iron concentration.

Srinivasulu *et al.* (2017) carried out XRD analysis of pure and Fe-doped ZnO thin films deposited by chemical spray pyrolysis. All the films showed peaks similar to pure ZnO, which indicated that no structural deformation occurred in ZnO lattice upon Fe-doping. A change in the preferred orientation from (002) to (101) plane was noticed while increasing the doping concentration ≥ 2 % that might be due to the presence of high Fe content in the films. It was also observed from the XRD patterns that the intensity of peaks was low at lower doping concentration ≤ 2 % and then increased.

Limaye *et al.* (2011) reported that the SEM characterization of lightly doped ZnO films showed a rough surface topography with tiny grains distributed over the smooth background. However, with increase of Fe-doping concentration, the grains were unevenly distributed with coarseness and

agglomeration of grains occurred due to the clustering of initial nuclei that led to formation of a compact film surface. Their UV-visible characterization showed that the undoped ZnO films had medium optical transmittance (> 70%) while the Fe-doped ZnO films with lower dopant concentration (≤ 2 %) exhibited slightly high optical transmittance (> 80%) than films with higher doping concentration (> 2 %) of iron.

The variation in the optical transmittance of the films in the visible region corresponds to the changes in both the crystalline quality and surface roughness of the films on Fe-doping. The evaluated band gaps were 3.24 eV, 3.28 eV, 3.26 eV, 3.13 eV and 3.01 eV for ZnO thin films with Fe concentration of 0%, 1%, 2%, 4% and 6 %, respectively (Limaye *et al.* (2011).

1.2 Statement of the problem

There have been few studies carried out on iron doped zinc oxide thin films as most studies are focused on doping zinc oxide with magnesium (Mg), aluminum (Al), cobalt (Co) or cadmium (Cd). Thus, the main issue that is intended to be addressed in this study is investigation of effect of iron on the electrical and optical properties of the zinc oxide thin films. Moreover, zinc oxide in its undoped form has the ability to absorb and emit only ultraviolet radiation in its band to band transitions. As a result it is only used in applications that require absorption or emission of UV radiations like in body lotions intended in protecting the skin from harmful UV radiation and in some cases in lasers that produce UV light. But it will be almost useless in applications that involve absorption or emission of radiations in lower energy spectrum such as visible or infrared regions. As a result the energy gap of zinc oxide needs to be reduced by introducing impurity states in order to make it useful in several other applications.

1.3 Significances of the study

The significance of this study is that it enables us to understand how iron modifies the optical and electrical properties of zinc oxide nanoparticles which in turn enable us to use these modifications to various applications. For instance introduction of iron in to zinc oxide results in the reduction of the energy band gap which makes it ideal for applications like photocatalyst and solar cells. Studies have reported the influence of iron doping in the structure of ZnO, revealing significant improvements in results with the metal addition, in applications such as photocatalysis and gas sensors. Iron is the most important dopant for ZnO because of its compatibility with Zn^{2+} ion, due to

its abundance and low cost, as well as its non-toxicity, which maintains the biocompatibility of ZnO particles, and also its ability to impart ferromagnetism to ZnO.

1.4 Objectives of the study

1.4.1 General objective

The general objective of this research is to study the electrical and optical properties of iron doped zinc oxide thin films grown by spin coating method for the use in optoelectronic devices.

1.4.2 Specific Objectives

The specific objectives of this study are to:

- synthesize pure and iron doped zinc oxide thin films using spin coating method,
- characterize the thin films using X-ray diffraction (XRD), photoluminescence (PL) and UV-visible spectroscopy,
- investigate the conductivities of the thin films using the result from Hall Effect measurements.

2. Literature Review

2.1 Structure and Properties of Zinc Oxide Nanoparticles

Zinc oxide, a well-known piezoelectric and electro-optic material with wide direct band gap (3.37 eV) and large exciton binding energy (60 meV), is now being considered as a potential material for a wide range of applications such as optoelectronic and luminescent devices as well as chemical sensors.

Generally, Zinc oxide crystallizes in two main forms, hexagonal wurtzite and cubic zinc blende as shown in Figure 1 (a) and (b). The wurtzite structure is most stable at environmental conditions and thus it is most common. The lattice constants of hexagonal wurtzite structure are $a = b = 3.25$ Å and $c = 5.2$ Å (Alver *et al*., 2007). By growing ZnO on substrates with cubic lattice structure, the zinc blende form can be stabilized. The lattice constant of ZnO in zinc blend structure is $a = b = c = 5.41$ Å (Hasanpoor *et al*., 2016). In both structures, the zinc and oxide centers are tetrahedral, which is the most characteristic structural geometry for zinc (Zn). In hexagonal and zinc blende polymorphs, there is no inversion symmetry, it means reflection of the crystals relative to any point do not alter it into itself. Other lattice symmetric properties consequence in piezo- and pyro-electric properties of hexagonal and zinc blende structures (Zegadi *et al*., 2015). Zinc Oxide nanoparticles have unique properties, which are summarized in table 1.

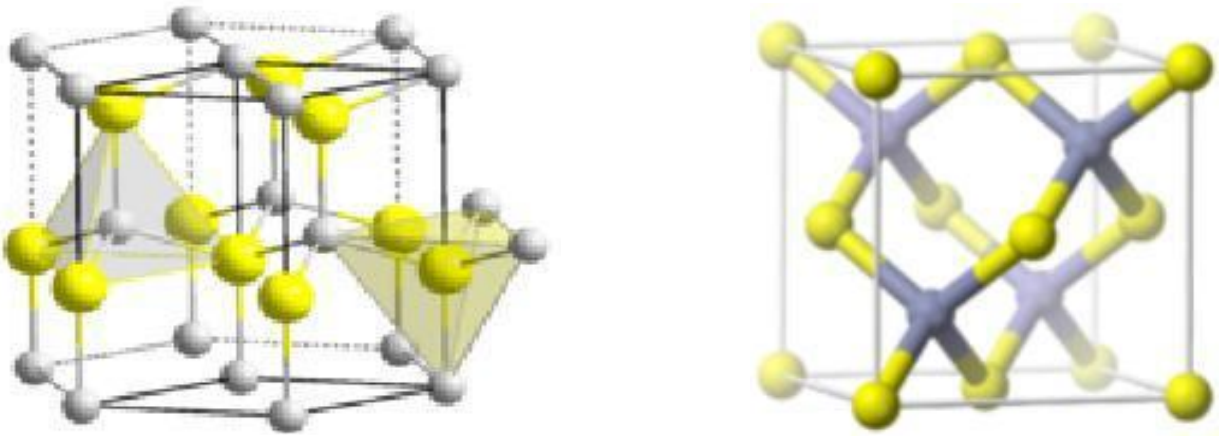

Figure 1: ZnO (a) hexagonal wurtzite and (b) zinc blende structure**s** (Alver *et al*., 2007).

Table 1: Basic Properties of Zinc Oxide nanoparticles (Alver *et al*., 2007).

1	Appearance	White solid
2	Odor	Odorless
3	Molecular Weight	81.38 g/mol
4	Most Common Crystal Structure	Wurtzite
5	Coordination Geometry	Tetrahedral
6	Lattice Constants	$a = 3.25$ Å , $c = 5.2$ Å
7	Band Gap	3.37 eV
8	Solubility in water	0.0004 % ($17.8\ ^{0}$c)
9	Refractive Index (µD)	2.0041
10	Density	5.606 g/cm^3
11	Melting Point	$1975\ ^{0}$c
12	Flash Point	$1436\ ^{0}$c

2.2 Doping of Zinc Oxide

Doping is the intentional introduction of impurities into an intrinsic semiconductor for the purpose of modulating its electrical, optical and structural properties. The doped material is referred to as an extrinsic semiconductor. A semiconductor doped to such high levels that it acts more like a conductor than a semiconductor is referred to as a degenerate semiconductor.

ZnO has a strong potential for various short-wavelength optoelectronic device applications. In order to attain the potential offered by ZnO, both high-quality n- and p-type ZnO are indispensable. However, difficulty in bipolar carrier doping (n and p-types) is a major obstacle as seen in other wide band gap semiconductors such as GaN and II-VI compound semiconductors including ZnS, ZnSe, and ZnTe (Reddy *et al*., 2012). Unipolar doping has not been a surprising issue in wide-band-gap semiconductors: ZnO, GaN, ZnS, and ZnSe are easily doped to n-type, while p-type doping is difficult. The situation is opposite for ZnTe where p-type doping is easily obtained, while n-type doping is difficult (Saleh *et al*., 2012).

2.2.1 n-type doping

ZnO with a wurtzite structure is naturally an n-type semiconductor because of the presence of intrinsic defects such as O vacancies (V_O) and Zn interstitials (Zn_i) (Sato & Katayama, 2001). Undoped ZnO shows intrinsic n-type conductivity with very high electron densities of about 10^{21} cm^{-3} (Singhal *et al*., 2008). Although it is experimentally known that unintentionally doped ZnO is n-type, whether the donors are Zn_i or V_O is still controversial. The first-principles study suggested that none of the native defects show high concentration shallow donor characteristics. However, some studies have suggested that Zn_i rather than V_O is the dominant native shallow donor in ZnO with an ionization energy of about 30–50 meV (Smith & Nie, 2010). It has also been suggested that the n-type conductivity of unintentionally doped ZnO films could be due to hydrogen atoms (H) which act as a shallow donor with ionization energy about 30 meV. This assumption is valid since hydrogen is always present in all growth methods and can easily diffuse into ZnO in large amounts due to its large mobility.

n-type doping of ZnO is relatively easy compared to p-type doping. Group-III elements Al, Ga, and In as substitutional elements for Zn and group-VII elements Cl and I as substitutional elements for O can be used as n-type dopants. Iron is also another element that can be used to obtain n-type zinc oxide. Doping with Al, Ga, and In has been attempted by many groups, resulting in high-quality, highly conductive n-type ZnO films (Maldonado *et al*., 2001). Such films are successfully used in various applications as n-type layers in light emitting diodes as well as transparent Ohmic contacts.

2.2.2 p-type Doping

As mentioned repeatedly it is very difficult to obtain p-type doping in wide band gap semiconductors, such as GaN and ZnSe. The difficulties can arise from a variety of causes. Dopants may be compensated by low energy native defects, such as Zn_i or V_O, or background impurities like hydrogen (Smith & Nie, 2010). Low solubility of the dopant in the host material is also another possibility. Deep impurity level can also be a source of doping problem, causing significant resistance to the formation of shallow acceptor level. Known acceptors in ZnO include group-I elements such as Li, Na, and K, Cu, Ag, Zn vacancies, and group-V elements such as N, P, and As (Mishra & Das, 2010). However, many of these form deep acceptors and do not contribute significantly to p-type conduction. It has been believed that the most promising dopants

for p-type ZnO are the group-V elements, although theory suggests some difficulty in achieving shallow acceptor level.

2.3 Zinc oxide for optoelectronic Devices

Optoelectronics (or optronics) is the study and application of electronic devices and systems that source, detect and control light, usually considered as a sub-field of photonics (Zhang *et al*., 2013). In this context, light often includes invisible forms of radiation such as gamma, x-ray, ultraviolet and infrared radiations, in addition to visible light. Optoelectronic devices are electrical to optical or optical to electrical transducers (Shinde *et al*., 2012). Some examples of optoelectronic devices are photodiodes, phototransistors, photomultipliers, photoresistors, light emitting diodes (LEDs) and solar cells.

Gallim nitride (GaN) is used as the major source for blue lasers since the mid-1990s (Mittiga et al., 2006). It is also used extensively in fabricating devices like piezoelectric and waveguide devices, light emitting diodes and photodetectors. However, ZnO has emerged as a possible competitor in opto electronic applications as the structure and the band gap of zinc oxide prove promising for these applications. Studies have proved that ZnO could be used as the substrate for GaN films as both the materials share the same structure. The exciton binding energy, the important property for any optical device like LEDs and lasers is 60 meV in ZnO, which is 2.4 times that of GaN (Gao *et al*., 2012; Raksa *et al*., 2009). This is the reason why ZnO is considered as a prospective candidate for these devices. Apart from these optical properties, ZnO has some interesting physical properties that have made it more attractive in this field. With a melting point of 2000 °C, it is sufficiently stable at high temperatures (Conibeer, 2007). This is an important requirement during doping and formation of ohmic contacts. The higher hardness, resistance to mechanical stress and high melting point temperature of a material also expand the lifetime of LEDs and blue laser diodes. Therefore, ZnO as a potential wide band gap material can be used in short wavelength light emitting devices such as light emitting diodes, photodetectors, electroluminescence devices and the next generation of UV semiconductor lasers (Lopez *et al*., 2011).

2.4 Methods of thin film deposition

There are various methods to synthesize thin film semiconductor on a substrate. These methods include, Solution processing (Spin coating and dip coating), Vapor deposition (Chemical and Physical), molecular Beam epitaxy, magnetron co-sputtering and chemical spray pyrolysis methods (Wadia *et al*., 2009). Here only spin-coating method will be discussed as it is this technique that has been employed in this study.

2.4.1 Spin Coating Method

Spin coating has been used for several decades for the application of thin films. A typical process involves depositing a small puddle of a fluid resin onto the center of a substrate and then spinning the substrate at high speed (typically around 3000 rpm) (Ashour *et al*., 2006). Centrifugal force causes the resin to spread to, and eventually off, the edge of the substrate leaving a thin film of resin on the surface. Final film thickness and other properties will depend on the nature of the resin (viscosity, drying rate, percent solids, surface tension, etc.) and the parameters chosen for the spin process. Factors such as final rotational speed, acceleration, and fume exhaust contribute to how the properties of coated films are defined (Monticone & Alexis, 1998; Fardousi et al., 2013).

A typical spin process consists of a dispense step in which the resin fluid is deposited onto the substrate surface, a high speed spin step to thin the fluid, and a drying step to eliminate excess solvents from the resulting film. Two common methods of dispense are Static dispense, and Dynamic dispense (Ferdaus *et al*., 2014). Static dispense is simply depositing a small puddle of fluid on or near the center of the substrate. This can range from 1 to 10 cm^3 depending on the viscosity of the fluid and the size of the substrate to be coated. Higher viscosity and or larger substrates typically require a larger puddle to ensure full coverage of the substrate during the high speed spin step.

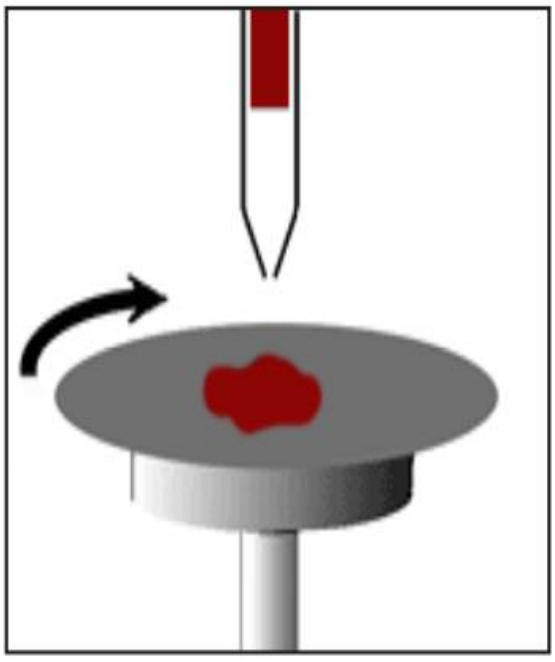

Figure 2: Spin coating method (Ferdaus *et al*., 2014).

Dynamic dispense is the process of dispensing while the substrate is turning at low speed. A speed of about 500 rpm is commonly used during this step of the process (Scriven, 2002). This serves to spread the fluid over the substrate and can result in less waste of resin material since it is usually not necessary to deposit as much to wet the entire surface of the substrate. This is a particularly advantageous method when the fluid or substrate itself has poor wetting abilities and can eliminate voids that may otherwise form. After the dispense step it is common to accelerate to a relatively high speed to thin the fluid to near its final desired thickness. Typical spin speeds for this step range from 1500-6000 rpm, again depending on the properties of the fluid as well as the substrate (Manikandan, 2015). This step can take from 10 seconds to several minutes. The combination of spin speed and time selected for this step will generally define the final film thickness.

2.5 Methods of Characterization

2.5.1 X-ray Diffraction (XRD)

X-ray crystallography (XRC) is the experimental science determining the atomic and molecular structure of a crystal, in which the crystalline structure causes a beam of incident X-rays to diffract into many specific directions (Alaa *et al*., 2017). By measuring the angles and intensities of these diffracted beams, a crystallographer can produce a three-dimensional picture of the density of electrons within the crystal. From this electron density, the mean positions of the atoms in the crystal can be determined, as well as their chemical bonds, their crystallographic disorder, and various other information (Brindley & Brown, 1980).

According to Bragg, diffraction occurs when radiation (with a wavelength comparable to atomic spacing) is scattered in a specular fashion by the atoms of a crystalline system, and undergoes constructive interference (Causin *et al*., 2010; Connolly, 2007). For a crystalline solid, the waves are scattered from lattice planes separated by the interplanar distance d. When the scattered waves interfere constructively, they remain in phase since the difference between the path lengths of the two waves is equal to an integer multiple of the wavelength. The path difference between two waves undergoing interference is given by $2d \sin\theta$, where θ is the diffraction angle. This leads to Bragg's law, which describes the condition on θ for the constructive interference to be at its strongest. Bragg's law is given as (Cullity, 1978):

$$2d \sin\theta = n\lambda, \tag{2.1}$$

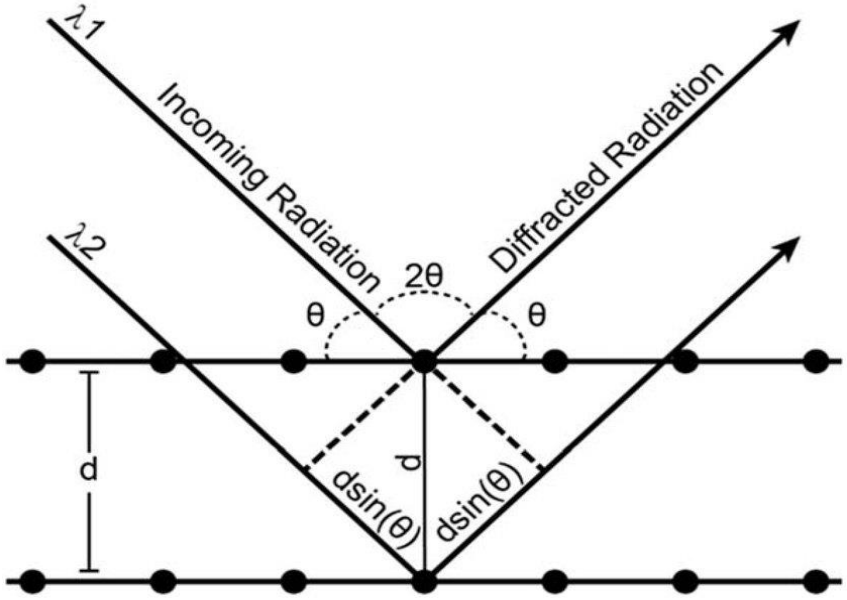

Figure 3: Bragg's law.

X-ray crystallography is still the primary method for characterizing the atomic structure of new materials and in discerning materials that appear similar by other experiments. X-ray crystal structures can also account for unusual electronic or elastic properties of a material, shed light on chemical interactions and processes, or serve as the basis for designing pharmaceuticals against diseases (Du *et al*., 2009). In a single-crystal X-ray diffraction measurement, a crystal is mounted on a goniometer. The goniometer is used to position the crystal at selected orientations. The crystal is illuminated with a finely focused monochromatic beam of X-rays, producing a diffraction pattern of regularly spaced spots known as reflections. The two-dimensional images taken at different orientations are converted into a three-dimensional model of the density of electrons within the crystal using the mathematical method of Fourier transforms, combined with chemical data known for the sample (Eckardt *et al*., 2012). Poor resolution (fuzziness) or even errors may result if the crystals are too small, or not uniform enough in their internal makeup. From XRD one can calculate the grain size using Scherrar's formula (Patterson, 1939).

$$D = \frac{0.94\lambda}{\beta \cos\theta'} \tag{2.2}$$

where λ is the wavelength of X-ray, θ is the Bragg's angle in degree and β is the full width at half maximum in radians. The lattice constants a and c of a hexagonal crystal structure are related by the following formula (Patterson, 1939):

$$a = \frac{1}{\sqrt{3}} \frac{\lambda}{\sin\theta}, \qquad c = \frac{\lambda}{\sin\theta}. \tag{2.3}$$

From a given XRD data one can also determine the dislocation density (δ) in lines/m^2 and lattice strain (ε) from the equations given bellow which tell us about the extent of the deformation caused by the dopants in the crystal structure and the mismatch between the polycrystalline film and the glass substrate respectively (Shakti & Gupta, 2010).

$$\delta = \frac{1}{D^2}, \qquad \varepsilon = \frac{\beta \cos\theta}{4}. \tag{2.4}$$

2.5.2 UV-Visible Spectroscopy

UV-Visible absorption spectroscopy is the measurement of the attenuation of a beam of light after it passes through a sample or after reflection from a sample surface (Perkampus, 2013). Absorption measurement can be done at a single wavelength (using monochromatic light) or over an extended spectra range. The principle of UV-Visible spectroscopy is based on the absorption of UV light or visible light by chemical compounds, which result in the production of distinct spectra. Spectroscopy is based on the interaction between light and matter. When the matter absorbs light, it undergoes excitation and de-excitation, resulting in the production of a spectrum of light (Brown & Palmer, 2009). When matter absorbs ultraviolet radiation, the electrons in it undergo excitation. This causes them to jump from a ground state to an excited state.

Visible and ultraviolet lights are energetic enough to promote outer electrons to higher energy levels and UV-Vis spectroscopy is used to find the absorbance, energy band gaps and intensity over wave length of molecules or inorganic complexes in solution (Giusti & Wrolstad, 2001). The UV-Vis spectra have broad features that are of limited use for sample identification but are very useful for quantitative measurements. The concentration of sample solution can be determined by measuring the absorbance at some wavelength. The Beer-Lambert law states that the absorbance of a solution is directly proportional to the concentration of the solution. This relation can be expressed as (Kutty, 2004):

$$I = I_0 e^{-\alpha x}, \tag{2.5}$$

where α is the measured absorption coefficient, I_0 is the intensity of the incident light at a given wavelength and I is the detected intensity at depth x. $\alpha = \varepsilon c$, where ε is molar absorptivity and c is concentration of the solution. The optical absorption coefficient can also be determined based on its dependence on the energy band gap(E_g). The energy band gap of the sample is obtained by using the absorption edge relation (Monticone & Alexsis, 1999).

$$E_g = \frac{hC}{\lambda} = \frac{1{,}240}{\lambda}\ eV, \tag{2.6}$$

where h is planck′s constant and C is the speed of light. For photon energies just above fundamental edge, the absorption coefficient follows the standard relation (Kutty, 2004):

$$\alpha h\upsilon = A\left(h\upsilon - E_g\right)^n, \qquad \alpha = \frac{4\pi k}{\lambda}, \tag{2.7}$$

where A is a constant related to the extent of the band tailing, k represents the imaginary part of the refractive index, $h\upsilon$ is photon energy, E_g is energy band gap which is the energy gap between the valence band and the conduction band and the value of n is $1/2$ for allowed direct transition and 2 for allowed indirect transition.

In addition to determining the energy band gap and absorbance of thin films, UV-Visible spectroscopy can be used to determine the thickness of thin films using Swaneopeol method which uses the equation (Monticone & Alexsis, 1999):

$$t = \frac{\lambda_1 \lambda_2}{2(\lambda_1 n_2 - \lambda_2 n_1)}, \tag{2.8}$$

where t is thickness, λ_1 and λ_2 are wavelengths of two successive peaks in the transmittance versus wavelength graph and n_2 and n_1 are refractive indices at λ_2 and λ_1 respectively. The refractive indices can be obtained using equation:

$$n = [\,N + (N^2 - S^2)^{\frac{1}{2}}]^{\frac{1}{2}}, \tag{2.9}$$

where

$$N = 2s\left(\frac{T_M - T_m}{T_M T_m}\right) + \frac{s^2 + 1}{2}. \qquad (2.10)$$

T_M and T_m are upper and lower bounds of the enveloped transmittance versus wavelength graph while s is a constant having a value of 1.51.

2.5.3 Photoluminescence (PL) Spectroscopy

Photoluminescence (PL) spectroscopy is a non-destructive analytical technique in which a material is illuminated with light, usually from a laser, and the resulting luminescence is recorded as a plot of emitted light intensity versus wavelength (Heiman, 2004; Kurbanov *et al*., 2010). Photoluminescence, the emission of visible light, occurs when an energy source (laser, UV lamp, etc.) knocks an electron out of its stable "ground" state and elevates it to an "excited" state. As the electron returns to its ground state, energy is released, much of it in the form of visible light as depicted in Figure 4. In almost all cases, the emitted light is of a lower energy in the electromagnetic spectrum than the original light from the energy source (Reynolds et al., 1998). Since wavelength and energy are inversely proportional, a lower energy always translates to a higher wavelength. Therefore, PL spectra always encompass a wavelength range that is higher than the wavelength of the excitation source. The relationship between energy (-eV) and wavelength (-nm) is given in equation (2.6).

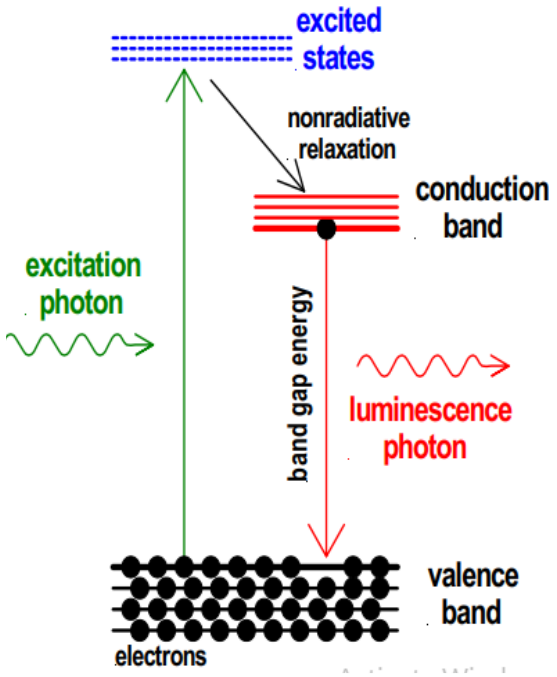

Figure 4: Principle of Photoluminescence Spectroscopy.

2.5.4 Hall Effect Measurement

In 1879 E. H. Hall observed that when an electrical current passes through a sample placed in a magnetic field, a potential proportional to the current and to the magnetic field is developed across the material in a direction perpendicular to both the current and to the magnetic field (Hall, 1879). This effect is known as the Hall Effect, and is the basis of many practical applications and devices such as magnetic field measurements, and position and motion detectors. With the measurements he

made, Hall was able to determine for the first time the sign of charge carriers in a conductor. Even today, Hall Effect measurements continue to be a useful technique for characterizing the electrical transport properties of metals and semiconductors. Figure 5 shows the working principle of Hall Effect measurements.

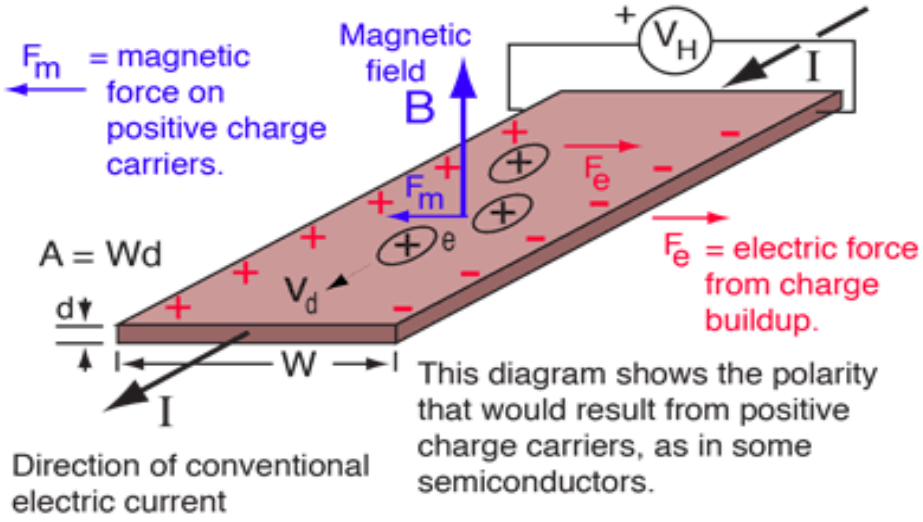

Figure 5: Principle of Hall Effect (Streetman & Banerjee, 2009).

Let's assume we applied magnetic field B_z in the z-direction on a semiconductor film of thickness t. If a current I_x is flowing in the x-direction inside the film, then the majority carrier density n_0, the drift velocity ϑ_d, the carrier mobility μ_n and the conductivity σ_n of the film can be calculated from Hall Effect measurement using the following formulas (Hall, 1879).

$$n_0 = -\frac{I_x B_z}{V_H e t}, \qquad \vartheta_d = \frac{I_x}{n_0 e w t}, \tag{2.11}$$

$$\mu_n = \frac{\vartheta_d}{E}, \tag{2.12}$$

$$\sigma_n = e n_0 \mu_n, \tag{2.13}$$

where w is the width of the sample, e is elementary charge, V_H is Hall voltage and E is magnitude of the electric field.

Temperature dependent Hall Effect measurement gives us several important electrical parameters of thin films as a function of temperature one of which is the majority carrier concentration. The majority carrier density in n-type semiconductor can be described in terms of the net donor ionization density, N_d^+ and the intrinsic carrier density, n_i as (Streetman & Banerjee, 2009):

$$n_0 = \frac{N_d^+}{2} + \sqrt{n_i^2 + \frac{N_d^{+2}}{4}}. \tag{2.14}$$

The ionization density, N_{di}^+ of the i^{th} shallow donor is given by (Shura, 2019):

$$N_{di}^+ = \frac{2N_{di}}{1 + \sqrt{1 + 4g_d \frac{N_{di}}{N_C} \exp\left(\frac{\Delta E_{di}}{k_B T}\right)}}, \tag{2.15}$$

where N_{di} is the density of the i^{th} shallow donor, ΔE_{di} is its activation energy, g_d is the spin degeneracy at the donor sites (only one parabolic band at the conduction band edge and thus $g_d = 2$) and N_C is the effective density of the conduction band state given in terms of the conduction band effective mass, m_n^* as (Blakemore, 1987):

$$N_C = 2\left(\frac{2\pi m_n^* k_B T}{h^2}\right)^{3/2}. \tag{2.16}$$

For a system with more than one shallow donors, the net donor ionization density, N_d^+ is given by the sum of the densities all the shallow donors in the system (Blakemore, 1998):

$$N_d^+ = \sum_i N_{di}^+. \tag{2.17}$$

When the value of the majority carrier obtained from the Hall Effect measurements in equation (2.11) is fitted with the theoretical description in equation (2.14), the dopant densities and the activation energies of the shallow dopants can be described easily.

3. Materials and Methods

3.1 Chemicals and Apparatuses

The chemicals used in this study were Zinc nitrate hexahydrate (Zn $(NO_3)_2.6H_2O$), sodium hydroxide (NaOH), iron nitrate nanohaydrate ($Fe(NO_3)_3.\ 9H_2O$), distilled water, and acetone (C_3H_6O). The apparatuses used in the experiment to synthesize thin films were: hot plate with magnetic stirrer, electronic balance, measuring cylinder, beakers, Oven, furnace, spin coater and microscopic glass substrate. UV-Visible Spectroscopy, X-ray diffractometer, photoluminescence spectroscopy and Hall Effect measurement devices have been used to characterize different aspects of the Fe-doped ZnO thin films.

3.2 Synthesis Procedures

0.5 M aqueous solution of Zn $(NO_3)_2.6H_2O$ was prepared by dissolving 12 gram of Zn $(NO_3)_2.6H_2O$ in 100 ml of distilled water in a beaker under magnetic stirring at 70 °c for 15 minutes. In a separate beaker, 3 gram of NaOH was dissolved in 50 ml of distilled water under magnetic stirring at 70 °c for 15 minutes to get 1.5 M solution. The solution of NaOH was slowly poured into the Zn $(NO_3)_2.6H_2O$ solution showing milky white color and was kept under constant stirring at 70 °c for 1 hour. The PH of the solution was adjusted to 9. The final solution was kept in dark place to avoid light assisted reaction and was aged for approximately 36 hours.

In another set of reaction 0.0125 M aqueous solution of $Fe(NO_3)_3.9H_2O$ was prepared by dissolving 0.253 gram of $Fe(NO_3)_3.9H_2O$ in 50 ml of distilled water under magnetic stirring for 15 minutes at 70 °c. 0.625 M of aqueous solution of Zn $(NO_3)_2.6H_2O$ was prepared by dissolving 18.594 gram Zn $(NO_3)_2.6H_2O$ in 100 ml of distilled water under magnetic stirring for 15 minutes at 70 °c. The first solution was slowly poured in to the second under constant stirring and the resulting solution was stirred for 1 hour at 70 °c. The Fe:Zn ratio was 1%. The PH of the solution was adjusted to 9 and kept in dark for 36 hours. This process was repeated three more times by dissolving 0.758, 1.263 and 2.53 grams of $Fe(NO_3)_3.\ 9H_2O$ in 50 ml of distilled water under magnetic stirring for 15 minutes to obtain 0.0375, 0.0625 and 0.125 M aqueous solutions of $Fe(NO_3)_3.9H_2O$ respectively. The concentration of Zn $(NO_3)_2.6H_2O$ was kept constant at 0.625 M. The Fe:Zn ratios were 3%, 5% and 10 %.

Once the necessary solutions were prepared and aged, microscopic glass substrate were cleaned using acetone and distilled water in UV sonicator and dried in ovens. The solutions were coated on the glass substrates using vacuum spin coater at 3000 rpm for 30 seconds. This process was repeated 10 times with each round being followed by 20 minutes of drying using hot plate to obtain the desired film thickness and crystal quality. Once the coating was done the obtained thin films were calcinated at 500 °c for 2 hours.

3.3 Characterization Procedures

The crystal structure of the prepared thin films were studied using XRD (Maxima, Shimazdu Corporation) with Cu Kα radiation ($\lambda = 1.540$ Å) in 2θ range of $10° - 80°$. The absorption and emission spectra of the films were studied using UV-visible (Perkin Elmer Lambda 19) and Photoluminescence Spectrometer (FLS1000) in the wavelength range of 250-900 nm and 350-600 nm respectively. The PL measurement was done using 330 nm as the excitation wavelength. The thickness of the samples was calculated using Swaneopeol method. The electrical properties of the thin films were studied using Hall Effect measurement device. The Hall Effect measurement was carried out using four probes with equal spacing which were brought in contact with four terminals constructed from silver paste on the thin films in the Vander Pauw configuration. Two of the probes fed the thin films with a constant current of 2 mA while the other two probes measured the potential drop across the films. A constant magnetic field of 0.556 T was used and the temperature was varied from 170-300 K with a step increment of 10 K.

4. Results and Discussion

4.1 X-ray Diffraction Analysis

The X-ray diffraction patterns of pure and Fe-doped ZnO films are as shown in Figure 6. It can be seen that all the grown films were polycrystalline in nature, showing multiple peaks corresponding to (100), (002), (101), (102), (103), (110), (112), (200) and (201) planes related to the hexagonal wurtzite crystal structure. All these observed peaks are very well matched with the peaks in the JCPDS card. Irrespective of doping concentration, all the films showed peaks similar to pure ZnO. This confirms the successful replacement of Fe ions in Zn lattice sites in the ZnO matrix. An initial shift in preferred orientation from (101) to (002) plane can be observed in the sample with iron concentration of 1%. However, the preferred orientation shifted back to (101) plane as the iron concentration was increased further. This result is slightly in agreement with the result obtained by Srinivasulu *et al.* (2017) in which they also observed the preferred orientation shifting from (002) to (101) as the concentration of iron increased.

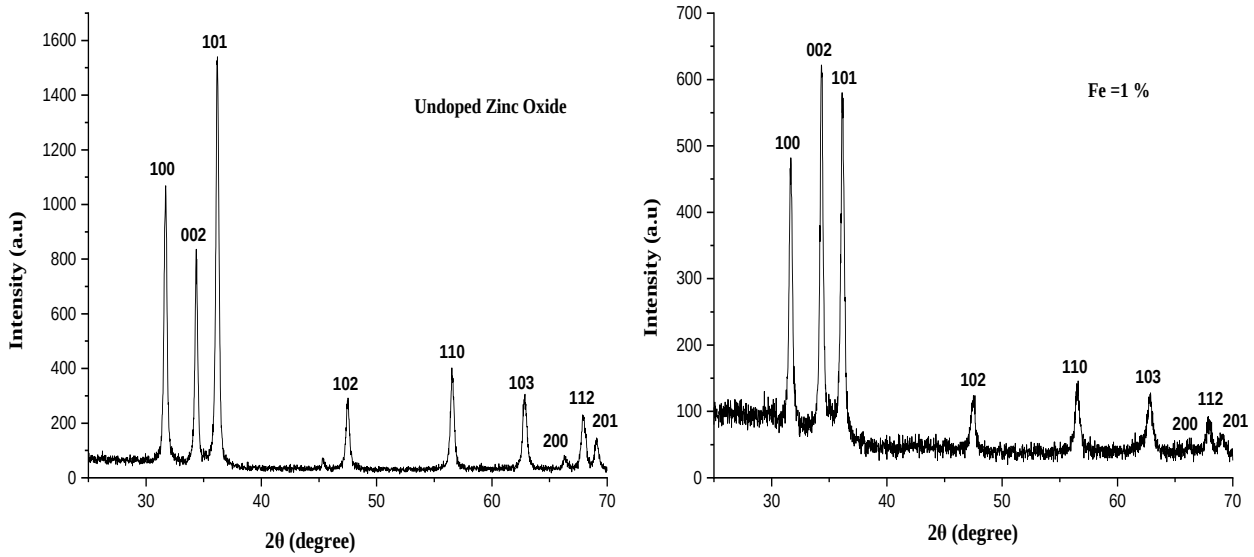

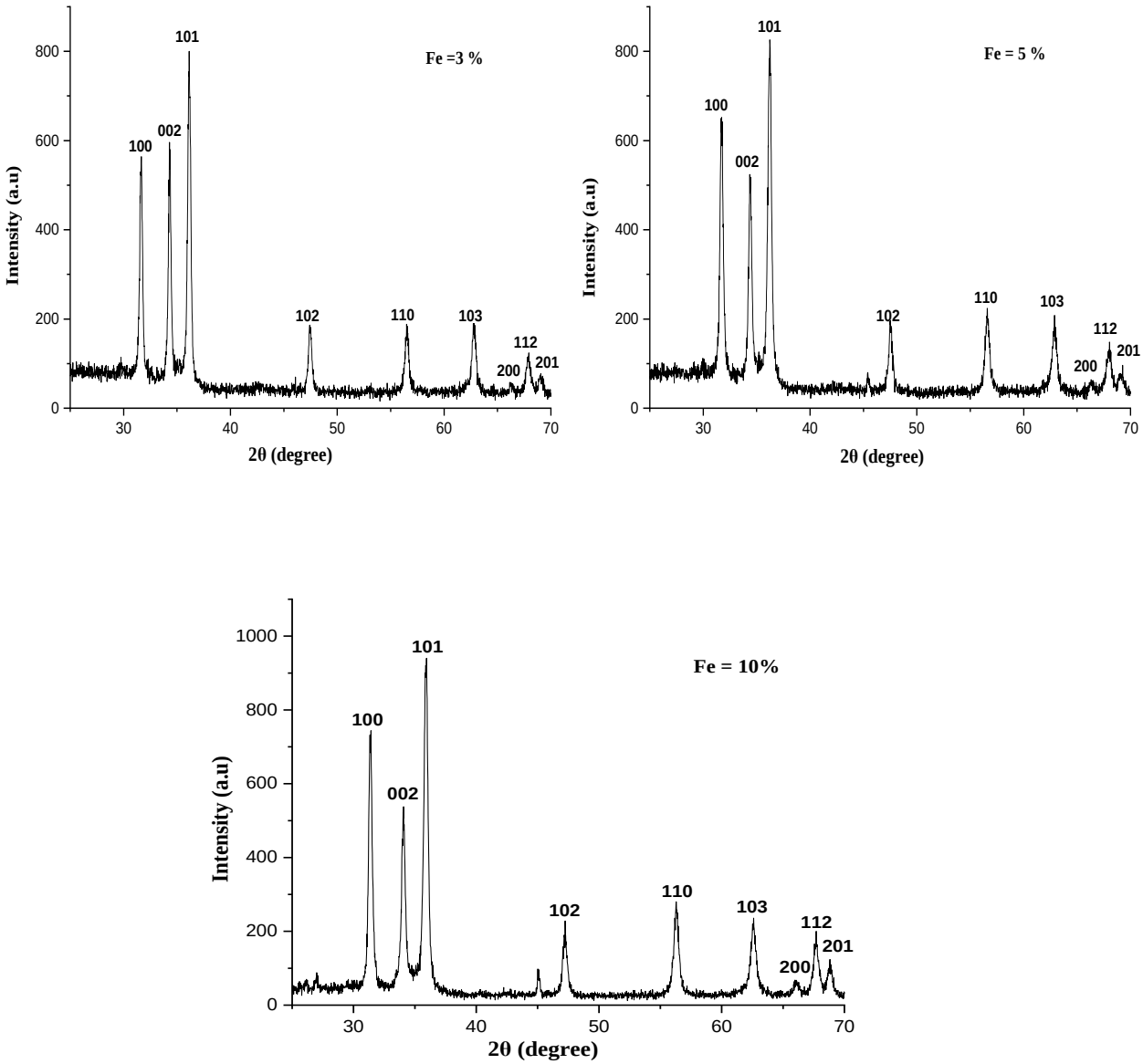

Figure 6: XRD peaks of zinc oxide thin films with different iron concentration of 0%, 1%, 3%, 5% and 10%.

It can also be observed from the XRD patterns that the intensity of peaks for the undoped zinc oxide film was very high. But, upon the introduction of iron in to it the intensity initially decreased and then increased as the concentration of the dopant was increased. This variation in peak intensity directly shows the impact of doping concentration on surface texture of the films. Similar increase of peak intensity with Fe-doping was observed by Rambu *et al.* (2013) for Fe-doped ZnO films deposited by spin coating technique. The intensities of various diffraction peaks are different, which

indicates that the growth of ZnO in various planes is different and the growth is anisotropic. Crystalline quality is degraded with the increase of Fe-content in the ZnO films resulting in decrease of transmittance. The lattice parameters such as lattice constants, grain size, lattice strain and dislocation densities were evaluated by using the appropriate formulae given in equation (2.2)-(2.4) as shown in the table below.

Table 2: Lattice parameters of zinc oxide thin films for different iron concentration.

Fe (%)	Crystal Plane (hkl)	Grain Size (nm)	$\delta \times 10^{14}$ (lines/m^2)	$\varepsilon \times 10^{-3}$	Lattice Constants (Å)	
					A	C
0	(101)	30.67	10.63	1.18	2.86	4.96
1	(002)	29.88	11.19	1.21	3.01	5.22
3	(101)	26.38	14.37	1.37	2.87	4.97
5	(101)	22.49	19.77	1.60	2.86	4.96
10	(101)	22.47	19.81	1.61	2.84	4.92

As it can be seen in the above table the lattice constants of the thin films increased slightly as the dopant concentration was increased to 1%. This is due the shift in the preferential plane from (101) to (002). However the lattice constants decreased as the concentration of iron was increased further. This is expected because of the misfit in the radii of the Fe^{+3} and Zn^{+2} ions when the replace of the latter by the former took place. As it is known the radius of Fe^{+3} ion is smaller than that of Zn^{+2}. Thus, when Fe^{+3} ions substitute Zn^{+2} ions in the zinc oxide matrix the lattice constants shrink. A similar behavior was reported by Mehedi *et al.* (2014). One can also observe that the grain size decreased considerably from 30.67 nm to 22.47 nm as the dopant concentration was increased. This is probably because of the large strain in the films which affects the normal growth of ZnO grains.

Moreover, the dislocation densities and lattice strains generally increased with increasing dopant concentration which indicates the formation of more and more defects due to addition of increasing amount of iron. This is because the iron ions added into the zinc oxide matrix don't always replace the zinc ions successfully as some of them can be locked in the interstitial places resulting in more crystal defects and charge imbalance around the dopants. The lowest values of dislocation density

and lattice strain indicate better crystal quality and less misfits between the substrates and the films. These values belong to the films with 0% and 1% iron as shown in the above table. Thus the film with iron concentration of 1% can be taken as optimal film.

4.2 Optical Analysis

The thicknesses of the thin films were found to be 2.496, 2.407, 2.450, 2.449 and 2.350 µm for 0%, 1%, 3%, 5% and 10% iron concentration. The absorbance spectra of the thin films were studied using the UV-vis spectroscopy and the results were plotted as shown in the Figure 7. From this figure one can observe that all the films except the undoped one have multiple absorption peaks. The main peaks at 374 and 380 nm are due to the transition of electrons from the valance to conduction band. On the other hand the peaks at 440, 443, 445 and 458 nm may correspond to the excitation of electrons from the valence band to the deep levels of oxygen vacancy. The peaks at 492, 493, 501 and 506 nm may correspond to the transitions of electrons from some impurity states such as deep acceptor levels to the deep levels of oxygen vacancy. Such multiple peaks were also obtained by Xiaojuan *et al*. (2014) at 390, 440, 490 and 523 nm. Moreover, the main peaks of the films moved toward higher wavelength (from ultraviolate region to visible region) as the iron concentration was increased from 0% to 10 %.

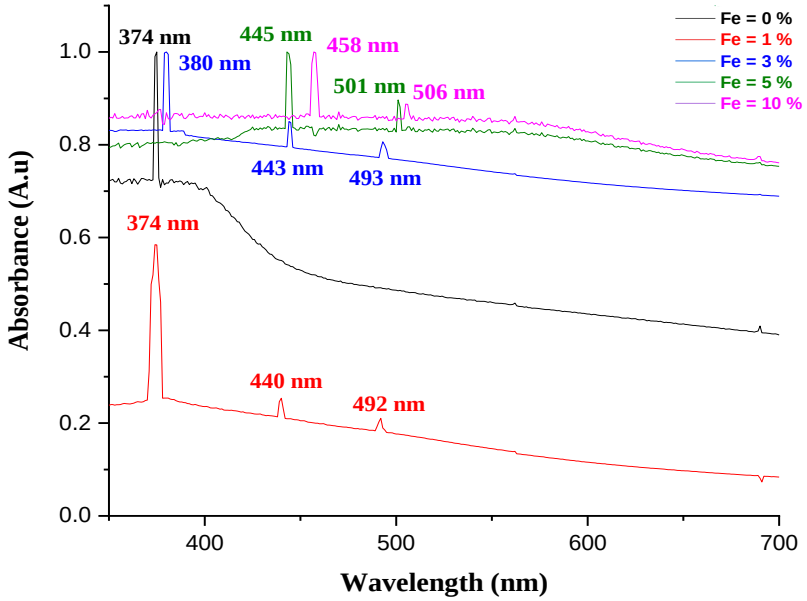

Figure 7: Absorbance versus wavelengths graph of zinc oxide thin films with different iron concentration.

Absorption peak wavelength tells us at what energy electrons in the crystal structure of the semiconductor undergo transitions from the valence band to the conduction band as well as impurity levels. According to this study the electrons in the undoped zinc oxide undergo band to band transitions after they absorb photons with energy in the ultraviolate region of the electromagnetic spectrum (i.e 374 nm or 3.3 ev). Upon doping zinc oxide with 1% of iron, the main absorption peak wavelengths did not change because the dopant concentration could have been small to make any significant change. But, peaks with low intensity appeared due to a possible excitation of small number of electrons from the valance band to the deep levels as well as from deep levels to the shallow donor levels. Upon increasing the concentration of iron to 3%, the density of the shallow donor levels increased and merged with the conduction band. This resulted in lowering of the conduction band minimum and effectively reducing the energy gap.

At the same time due to the increasing dopant concentration, the density of the deep levels of the oxygen vacancies increased resulting in more and more electronic transitions from valence band to the deep levels. This can be seen in the increase of the intensity of the small peaks. When the dopant concentration was increased to 5% and then to 10%, the density of the deep levels increased significantly making the electronic transition from the valence band to the deep levels dominant. This resulted in shift of the main peak of 5% and 10% iron doped zinc oxide thin films to higher wavelength. Thus, the electrons in the Fe-doped zinc oxide films of 3%, 5% and 10% iron can be excited from the valence band to the deep levels or the conduction band after absorbing photons with energy equal to that of violate and blue light.

As shown in Figure 8 the energy gap decreased from the initial value of 3.29 eV for undoped zinc oxide to 3.25 eV for Fe-doped zinc oxide of 3% iron. Similar decrease in band gap from 3.29 to 3.23 eV with increasing iron concentration was obtained by Cheng and Ma (2009). This decrease in energy gap can be attributed to the fact that new impurity levels are introduced close to the conduction band in the energy gap upon doping. When some Fe^{+3} ions substitute Zn^{+2} ions in the crystal lattice extra electrons are introduced with very small ionization energy. These electrons introduce impurity levels (which in this case are called shallow donor levels) close to the conduction band. When the concentration of the dopant increased the number of the extra electrons increases which in turn increase the density of the shallow donor levels near the conduction band.

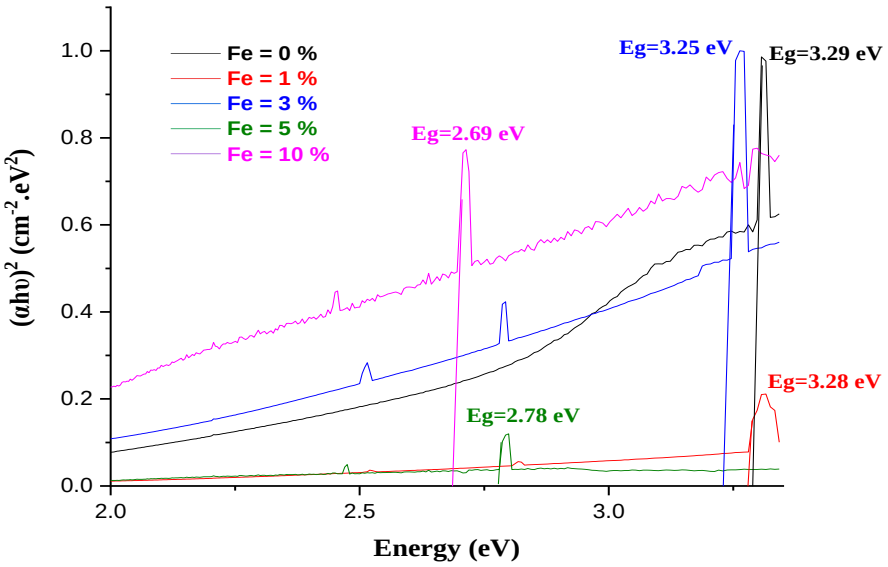

Figure 8: Tauc plot of zinc oxide thin films with different iron concentration.

This increase in density of the donor levels result in the overlapping of the conduction band and the shallow donor levels which effectively reduce the energy gap. Increasing iron concentration to 5% and 10 % results in more and more formation of oxygen vacancies due to the tendency of iron ions to form dimers in which each Fe^{+3} shares one oxygen with the other Fe^{+3}. Dimers are short chains of iron oxide units in which the iron ion doped into the ZnO removes one oxygen ion from the lattice to form chains creating oxygen vacancies. These oxygen vacancies introduce deep donor levels due to their ability to give electrons to the conduction band. Thus, increasing iron concentration results in increasing deep level density which means dominant electronic transitions from the valence band to these levels after absorbing visible light.

The photoluminescence study of the films is shown in figure 10. The undoped zinc oxide film has an emission peaks at 377 nm. The film with iron concentration of 1% has three peaks with the main peak appearing at 379 and the other two appearing at 445 and 495 nm. The film with iron concentration of 3% also has three peaks at 380 (the main peak), 448 and 499 nm. The last two film have peaks at 447 (main peak) and 506 nm for 5% iron and 461(main peak) and 509 nm for 10% iron.

From the photoluminescence emission spectra shown in the graph above one can see there is a red shift in the emission peaks compared to the absorption peaks of the films from UV-vis study. Similar red shift was also obtained by Xiaojuan *et al*. (2014). The reason behind these red shifts can

be attributed to presence of lattice vibration (phonons) in the crystal structure of the films which make the electrons to relax from some excited state to lowers energy state inside the conduction band before they undergo transitions to the valence band or deep donor levels. This causes the emitted radiation to have lower energy than the absorbed radiation which in turn results in increasing of the wavelength of the emission peaks.

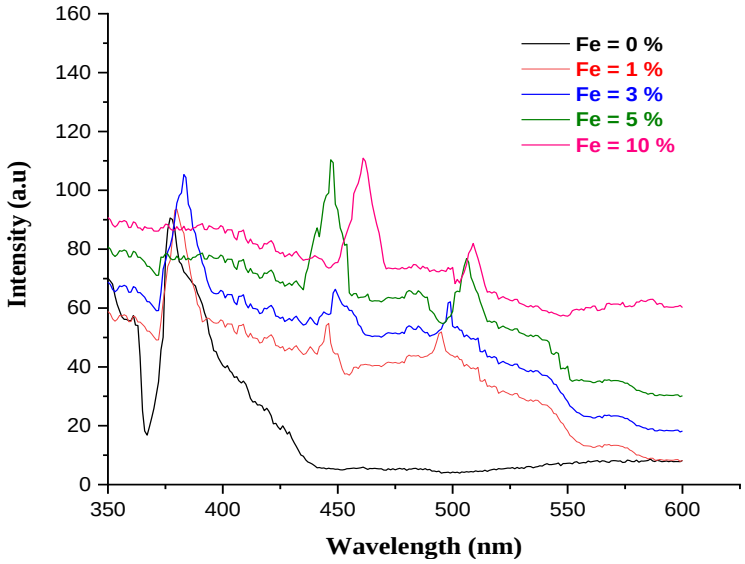

Figure 9: Emission intensity versus wavelength graph of undoped and Fe-doped zinc oxide thin films.

4.3 Hall Effect Analysis

The majority carrier concentration with varying temperature was measured and its behavior as a function of temperature was plotted as shown in Figure 10. As one can see from the graph the dotes represent the measured values of the carrier concentration at different temperature. The green and blue lines represent the calculated values of the shallow and deep donor level densities respectively for low and high temperatures. The red line represents the measured carrier concentration due to both shallow and deep donor levels extrapolated to low and high temperatures. This carrier concentration was fitted to the theoretical value using equation (2.15) and (2.14) by setting the intrinsic carrier density zero for both shallow and deep donor levels and summing up the resulting values.

The shallow donor levels in undoped ZnO thin film could be due to the already existing Zn interstitials (Zn_i) and impurities such as hydrogen atom while the deep levels could be due to oxygen vacancies formed during calcination in which the high temperature removes the oxygen ions in the form of oxygen molecules. The shallow donor level density of the films with 1%, 3%, 5% and 10 % iron was observed to increase initially but decrease subsequently due to different successes rate of substitution of zinc by iron from sample to sample. The more successful the replacement is the higher shallow donor density there will be. The shallow levels in all samples have activation energy less than 5 meV.

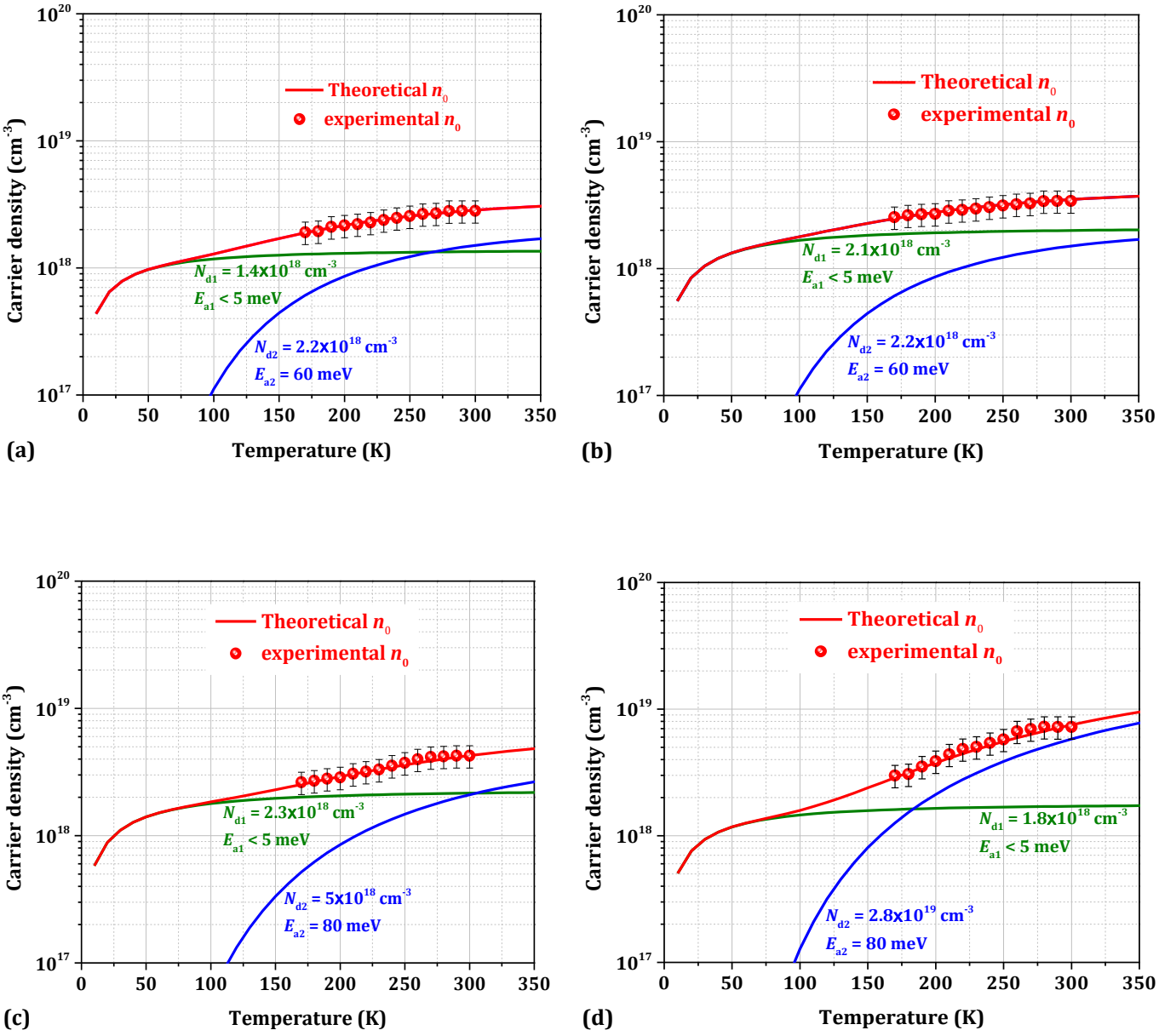

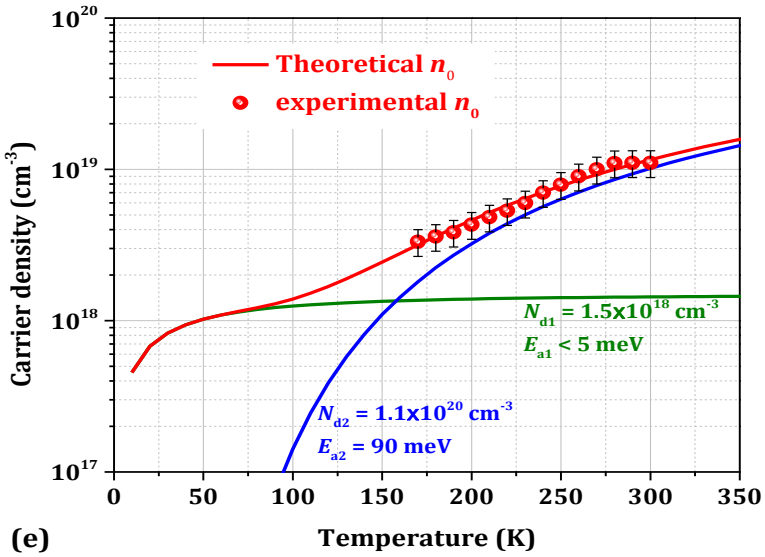

Figure 10: Carrier concentration versus temperature plot of zinc oxide thin films with (a) 0 %, (b) 1 %, (c) 3 %, (d) 5 % and (e) 10 % iron.

The deep level density on the other hand increased with increasing iron concentration due to more and more creation of oxygen vacancies. The depth of these deep levels also increased from 60 to 90 meV as the iron concentration was increased. The carrier concentration due to both shallow and deep donor levels increased with increasing temperature and iron concentration. This is in accordance to the relation given in (2.15) in which increasing temperature decreases the denominator which in turn increases the deep ionization densities. This in turn results in increase of the carrier concentration as given in relation (2.14). This increase in the carrier concentration can be attributed only to the deep levels as the shallow levels were already completely ionized when the measurement was carried out. However, the increase in the concentration slowed down as the temperature approaches room value. If the temperature is increased further, the concentration would start to approach a constant value indicating complete ionization of the deep levels. Thus, we can see that the temperature range used in this measurement is complete ionization region for the shallow donor levels while it is partial ionization region for the deep donor levels.

As shown in Figure 11 the conductivity of each film increased with both increasing temperature and dopant concentration. The reason behind this increment in conductivity is due to the fact that the carrier concentration in the conduction band increases with increasing temperature as more and more electrons are excited from the deep levels to the conduction band. Increased temperature means increased energy which means there is enough energy that can be accessible to the electrons

in the deep levels to jump from these localized states and becomes free charge carriers in the lattice structure of the films.

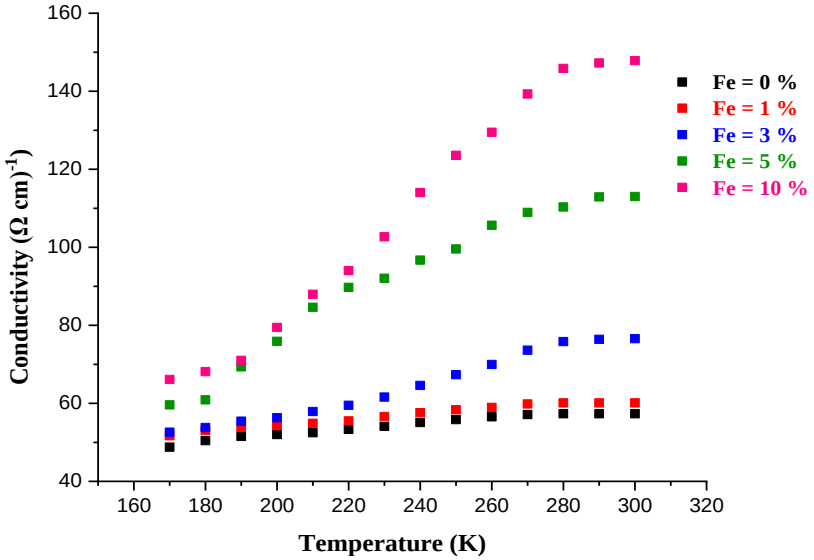

Figure 11: Conductivity versus temperature plot of zinc oxide thin films with different iron concentration.

This results in the observed enhancement of conductivity in the samples. However, the conductivity increased very slowly as the temperature approaches room value due very small increase in carrier concentration as we approach this temperature. Increasing the temperature beyond the room temperature might result in a further small increment in conductivity which eventually decrease when the temperature passes over the complete ionization region due to increased lattice vibration.

While the conductivity of the samples increased with increasing temperature and iron concentration, the mobility and sheet resistance decreased with increasing temperature and iron concentration as shown in Figure 12 and Figure 13. The reason behind the observed decrease in mobility with increasing temperature can be attributed to the increase in lattice vibration which impend the movement of the carriers. The increase in temperature results in high lattice and charge carrier vibration which increases the probability of the carrier-carrier as well as carrier-lattice collisions. These collisions cause the mobility to decrease as shown in Figure 12. On the other hand the decrease in mobility with increasing dopant concentration was due to the increment in carrier concentration which in turn created little free space in the lattice structure for the movement of the charge carriers. The above result is in agreement with the result obtained by Yang (2008) in which the mobility decreased above 160 K.

One might ask why didn't the conductivity decrease, just like the mobility, due to high lattice vibration. The answer would be that the large increase in carrier concentration outweighed the effect of lattice vibration. As we know conductivity is dependent on both the concentration and mobility of charge carriers as given in equation (2.13). But, the magnitude with which the concentration increased is far more larger than the magnitude with which the mobility decreased. As a result the conductivity increased despite increasing carrier-carrier and carrier-lattice collisions.

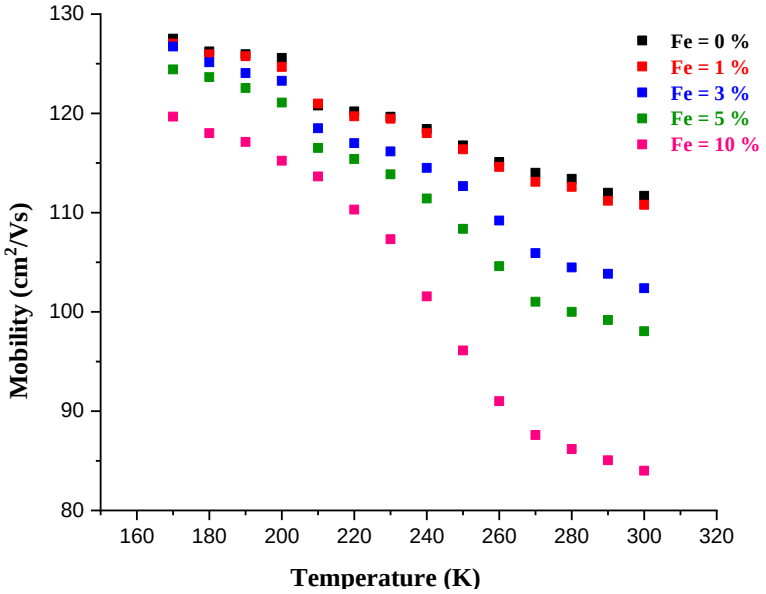

Figure 12: Mobility versus temperature plot of zinc oxide thin films with different iron concentration.

Just like the mobility the sheet resistance also decreased with increasing temperature and dopant concentration as shown in figure 14 due to increasing carrier concentration. Resistance and conductivity are reciprocal quantities of one another and as a result it is natural for the sheet resistance to decrease with increasing temperature and iron concentration. But as the temperature approaches room value it was observed to decrease very slowly due to slow increase in conductivity as discussed previously.

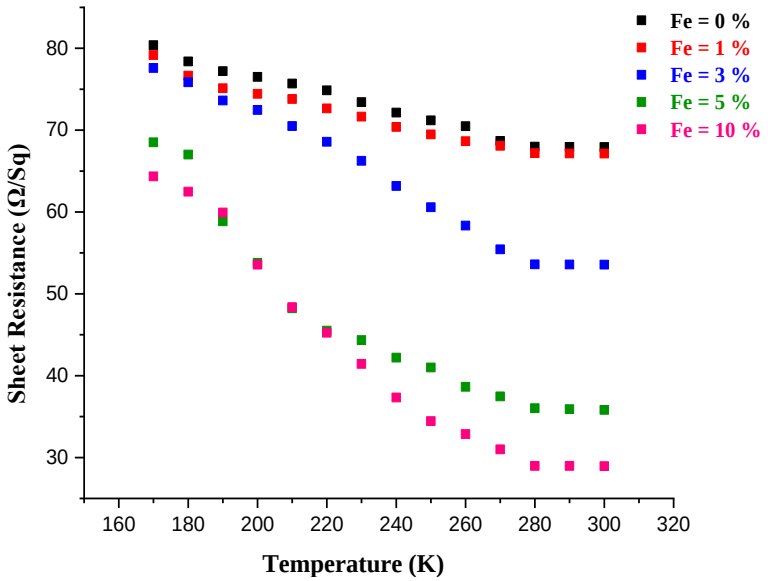

Figure 13: Sheet resistance versus temperature plot of zinc oxide thin films with different iron concentration.

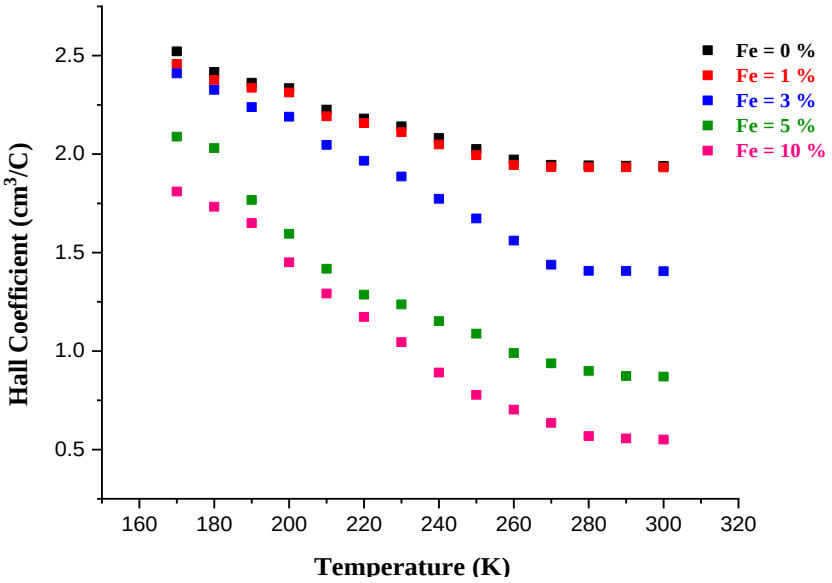

Figure 14: Magnitude of Hall coefficient versus temperature plot of zinc oxide thin films with different iron concentration.

Figure 14 shows dependence of hall coefficient on temperature and dopant concentration. As we can see the hall coefficient decreased with increasing temperature and iron concentration which can be attributed to the increase in carrier concentration. Since hall coefficient is the reciprocal of the total charge it falls as the total charge increase. But it can be see that the Hall coefficient starts to fall very slowly as it approaches room temperature. This can be due to small increment in the carrier

concentration as the temperature approaches complete ionization region of the deep levels. The approximate room temperature values of the parameters discussed in the Hall effect analysis so far are given in the table below.

Table 3: Room temperature electric parameters of zinc oxide thin films with different iron concentrations.

Fe (%)	n_0 **(cm^{-3})**	σ_n **(Ω cm)$^{-1}$**	μ_n **(cm^2/Vs)**	**Sheet Res. (Ω/sq)**	R_H
0	2.81x10^{18}	57.32	111.69	67.93	-1.94
1	3.41x10^{18}	60.12	110.78	67.13	-1.93
3	4.24x10^{18}	76.56	102.38	53.56	-1.41
5	7.24x10^{18}	112.99	98.05	35.82	-0.55
10	1.01x10^{19}	147.83	84.00	28.94	-0.54

The mobility obtained in this study was higher than the maximum mobility obtained by Navid *et al*. (2011) for aluminum doped zinc oxide thin films at room temperature, which was found to be 7.56 cm^2/Vs but the conductivity of their samples had higher values which was 161.81 (Ω cm)$^{-1}$. The conductivity and mobility of the samples obtained in this study showed practically acceptable values making them good candidates for optoelectronic applications.

5. Conclusion

In this study zinc oxide thin films doped with 0%, 1%, 3%, 5% and 10 % iron were grown on microscopic glass slides using spin coating method and calcinated at 500 °c for 2 hours. Structural study of the thin films showed growth of polycrystalline zinc oxide thin films with hexagonal wurtzite crystal structure on glass substrates. Successful substitution of zinc ions by iron ions was confirmed by the slight decrease in lattice constants. It was observed that crystal quality deteriorated with increasing iron concentration as revealed in increasing dislocation density and lattice strains which in turn resulted in decreased grain size. The optical study showed that enhanced absorption and emission spectra of the thin films over the visible light range was obtained with increasing iron concentration. The films with 3% iron showed ability to absorb visible light (violate) due to band gap reduction while the one with 5% and 10% iron showed the ability to absorb blue light due to deep donor levels of oxygen vacancies induced by increased iron concentration. The Hall measurement revealed that the electron mobility and sheet resistance decreased while conductivity and free electron density increased with increasing iron concentration and temperature. Over all, iron concentration of 3% can be taken as the optimum doping concentration for optoelectronic applications due to its relatively lower defects, good visible light absorption quality as well as good electron conductivity and mobility.

Research Fund Acknowledgment

This research project is funded by Adama Science and Technology University under the grant number ASTU/SM-R/258/21, Adama, Ethiopia.

Reference

Alaa, A.F., Suhayla, H., Zuha, W., & Hasan, W. (2017). Transparent solar cell using spin coating and screen printing. *Pertanika journal of science and technology*, *251*(4), 225-234.

Alver, U., Kilinc, T., Bacaksiz, E., & Nezir, S. (2007). Structural and optical properties of $Zn_{1-x}Fe_xO$ thin films prepared by ultrasonic spray pyrolysis. *Materials Science Engineering, 138*(31), 74–77.

Ashour, A., Kaid, M.A., El-Sayed, N.Z., & Ibrahim, A.A. (2006). Physical properties of ZnO thin films deposited by spray pyrolysis technique. *Applied Surface Science, 452*(2), 844–848.

Blakemore, J.S. (1987). *Semiconductor Statistics*. Dover Publications, New York.

Blakemore, J.S. (1998). *Solid state physics (2nd ed.)*. Cambridge University Press, New York.

Brindley, G. W., & Brown, G. (1980). Crystal Structures of Clay Minerals and Their Identification. *Mineralogical Society*, *123*(14), 99-106.

Brown, J.Q., & Palmer, G.M. (2009). Advances in quantitative UV–visible spectroscopy for clinical and pre-clinical application in cancer. *Journal of Physics: Condensed Matter*, *201*(10), 310-317.

Causin, V., Marega, C., Marigo, A., & Ripani, L. (2010). Forensic Differentiation of Paper by X-ray Diffraction and Infrared Spectroscopy. *Forensic Science International, 197*(16), 70–74.

Cheng, W., & Ma, X. (2009). Structural, optical and magnetic properties of Fe-doped ZnO. *Journal of Physics: Applied Physics*, *152*(9), 245-266.

Conibeer, G. (2007). Third-generation photovolatics. *Materials Today*, *10*(2), 142-150.

Connolly, J. R. (2007). Introduction to X-Ray Powder Diffraction. *Spring*, *142*(20), 124-130.

Cullity, B. D. (1978). *Elements of X-ray Diffraction(2nd ed.)*. Addison-Wesley, Menlo Park, CA.

Du, J., Benmore, C. J., Corrales, R., Hart, R. T., & Weber, J. K. (2009). Molecular Dynamics Simulation Interpretation of Neutron and X-ray Diffraction Measurements on Single Phase Y_2O_3-Al_2O_3 Glasses. *Journal of Physics: Condensed Matter*, *21*(3), 20–24.

Eckardt, R., Krupicka, E., & Hofmeister, W. (2012). Validation of Powder X-ray Diffraction Following. *Journal of Forensic Science, 57*(2), 722–737.

Fardousi, M., Hossain, M.F., Islam, M.S., & Ruslan, S. (2013). Cost-Effective Home-Made Spin Coater for Depositing Thin Films. *Journal of Modern Science and Technology, 1*(10), 126-134.

Ferdaus, M.,. Rashid, M.M., & Rahman, M. (2014). Design and Fabrication of a Simple Cost Effective Spin Coater for Deposition of Thin Film. *Advances in Environmental Biology*, *8*(4), 729-733.

Gao, F., Liu, X. J., Zhang, J. S., Song, M., & Li, N. (2012). Photovoltaic properties of the p-CuO / n-Si heterojunction prepared through reactive magnetron sputtering. *Journal of Applied Physics, 111*(8), 245-249.

Giusti, M.M., & Wrolstad, R.E. (2001). Characterization and measurement of anthocyanins by UV-visible spectroscopy. *Journal of physical chemistry A, 122*(11), 257-260.

Hall, E.H. (1879). On a new action of the magnet on electric currents. *American Journal of Mathematics, 3*(1), 287–292.

Hasanpoor, M., Aliofkhazraei, M., & Delavari, H. (2016). In-situ study of mass and current density for electrophoretic deposition of zinc oxide nanoparticles. *Ceramics International, 42*(33), 6906-6913.

Heiman, D. (2004). Photoluminescence. *Physics of Waves and Optics, 600*(24), 140-146.

Kaphle, A., Reed, T., & Hari, P. (2004). The Influence of Doping with Transition Metal Ions on the Structure and Magnetic Properties of Zinc Oxide Thin Films. *Journal of Applied Physics, 95*(21), 407-412.

Kripal, R., Gupta, A., Srivastava, R., & Mishra, S. (2011). Photoconductivity and photoluminescence of ZnO nanoparticles synthesized via co-precipitation method. *Spectrochimica Acta Part A: Molecular and Biomolecular Spectroscopy*, *79*(14), 1605-1612.

Kurbanov, S.S., Igamberdiev, K.T., & Kang, T.W. (2010). The UV laser induced heating effect on photoluminescence from ZnO nanocrystals deposited on different substrates. *Journal of Physics D: Applied Physics*, *43*(9), 115-121.

Kutty, N.M. (2004). UV-Visible spectroscopy. *Journal of Physics: Condensed Matter*, *321*(45), 301-309.

Limaye, M. (2011). Room temperature ferromagnetism in undoped and Fe doped ZnO nanorods: microwave-assisted synthesis. *Journal of Solid State Chemistry*, *184*(41), 391–400.

López, N., Reichertz, L. A., Yu, K. M., Campman, K., & Walukiewicz, W. (2011). Band structure for multiband solar cells. *Physical Review*, *106*(54), 415-421.

Magar, P., Kadam, V., Mulla, S., & Shaikh, V. (2009). Intrinsic and extrinsic origins of room temperature ferromagnetism in Fe-doped ZnO films. *Journal of Physics: Applied Physics*, *42*(11), 200-210.

Maldonado, A., Olvera, M.L., Asomoza, R., & Tirado, S. (2001). Chromium doped ZnO thin films deposited by chemical spray: chromium effect. *Journal of Vacuum Science & Technology A*, *18*(3), 2097–2101.

Manikandan, N. (2015). Construction of Spin Coating Machine Controlled by Arm Processor forPhysical Studies of PVA. *Environmental Science & Technology*, *323*(71), 123-129.

Mehedi, M., Khan, W., Azam, A., & Naqvi, A.H. (2014). Effect of size reduction on structural and optical properties of ZnO matrix due to successive doping of Fe ions. *Journal of Luminescence*, *145*(89), 160–166.

Mishra, A.K., & Das, D. (2010). Investigation on Fe-doped ZnO nanostructures prepared by a chemical route. *Materials Science and Engineering: B*, *171*(71), 415–420.

Mittiga, A., Salza, E., Sarto, F., Tucci, M., & Vasanthi, R. (2006). Heterojunction solar cells with 2% efficiency based on a Cu2O substrates. *Journal of Applied Physics* , *88*(24), 645-651.

Monticone, R., & Alexsis, S. (1998). The theory of spin coating method. *Journal of physical chemistry B, 102*(12), 218-524.

Monticone, R., & Alexsis, S. (1999). Complex nature of the UV and visible fluorescence of colloidal ZnO nanoparticles. *Journal of physical chemistry B, 112*(17), 600-604.

Muslih, E., & Munir, B. (2004). Optical and Magnetic Properties of ZnO nanoparticle. *Crystal Research Technology, 39*(6), 980-991.

Navid, M., Jahed, S., & Sivoththaman, S. (2011). Systematic control of carrier concentration and mobility in RF sputtered ZnO/Al:ZnO thin films. *Journal of Nanomaterials, 245*(5), 104-110.

Patterson, A.L. (1939). The Scherrer formula for X-ray particle size determination. *Physical Review, 56*(10), 978–982.

Pearton, S., & Liu, X. (2007). ZnO doped with transition metal ions. *Journal of Solid State Chemistry, 54*(16), 1040–1048.

Perkampus, H.H. (2013). UV-VIS Spectroscopy and its Applications. *Journal of Forensic Science, 145*(19), 515-520.

Pradeev, K., Sadaiyandi, K., & Kennedy, A. (2007). Synthesis and characterization of Fe-doped ZnO thin films deposited by chemical spray pyrolysis. *Applied Surface Science, 253*(23), 290-300.

Raksa, P., Nilphai, S., Gardchareon, A., & Choopun, S. (2009). Copper oxide thin films and nanowire as a barrier in ZnO dyesensitized solar cells. *Thin Solid Films, 517*(54), 741-744.

Rambu, A., Nica, V., & Dobromir, M. (2013). Influence of Fe-doping on the optical and electrical properties of ZnO films. *Superlattices Microstructure, 59*(7), 87–96.

Reddy, J.A., Kokila, M.K., Nagabhushana, H., Sharma, S.C., Rao, J.L., Nagabhushana, B.M. , Chakradhar, R.P., & Shivakumara, C. (2012). Structural, EPR, photo and thermoluminescence properties of ZnO:Fe nanoparticles. *Materials Chemistry and Physics, 133*(80), 876–883.

Reynolds, D.C., Look, D.C., Jogai, B., Nostrand, J.E., Jones, R., & Jenny, J. (1998). Source of the yellow luminescence band in GaN grown by gas-source molecular beam epitaxy and the green luminescence band in single crystal ZnO. *Solid State Community, 106*(46), 701–704.

Saleh, R., Prakoso, S.P., & Fishli, A. The influence of Fe doping on the structural, magnetic and optical properties of nanocrystalline ZnO particles. *Journal of Magnetism and Magnetic Materials*, *324*(64), 665–670.

Sato, K., & Katayama, H. (2001). Stabilization of ferromagnetic states by electron doping in Fe, Co or Ni-doped ZnO. *Japanese Journal of Applied Physics*, *40*(31), 334–336.

Scriven, L.E. (2002). Physics and applications of dip coating and spin coating. *International Journal of Electronics and Electrical Engineering, 121*(74), 789-792.

Shakti, N., & Gupta, P.S. (2010). Structural and optical properties of sol-gel prepared ZnO thin film. *Applied Physics Research, 2*(21), 19–28.

Shinde, S., Haranath, D., & Bhosale, C. (2012). Structural optoelectronic, luminescence and thermal properties of Ga-doped zinc oxide thin films. *Applied Surface Science, 258*(63), 969-976.

Shura, M. W. (2019). Investigation of dopant centres dominating the conduction process in the bulk of un-doped GaSb. *Journal of Theoretical and Applied Physics, 8*(5), 317-319.

Singhal, A., Acharya, S.N., Tyagi, A.K., Manna, P.K., & Yusuf, S.M. (2008). Colloidal Fe-doped ZnO nanocrystals: facile low temperature synthesis, characterization and properties. *Materials Science and Engineering: B, 153*(46), 347–352.

Smith, A.M., & Nie, S. (2010). Semiconductor nanocrystals: structure, properties, and band gap engineering. *Accounts of Chemical Research, 43*(4), 190–200.

Srikant, V., & Clarke, D. (1998). Structural, optical and magnetic properties of ZnO. *Journal of Applied Physics, 83*(21) , 504-510.

Srinivasulu, T., Saritha, K., & Ramakrishna, K.T. (2017). Synthesis and characterization of Fe-doped ZnO thin films deposited by chemical spray pyrolysis. *Modern Electronic Materials, 3*(1), 760–766.

Streetman, B.G., & Banerjee, S.K. (2009). *Solid State Electronic Devices (6th edn.)*. Asoke K. Ghosh, PHI Learning P. L., New Delhi.

Wadia, C., Alivisatos, A., Duniel, P., & Kammen, M. (2009). Materials availability expands the opportunity for large-scale photovoltaics deployment. *Environmental Science & Technology*, *43*(12), 207-2014.

Xiaojuan, W., Zhiqiang, W., Zhang, L., Wang, X., Yang, H., & Jiang, J. (2014). Optical and Magnetic Properties of Fe Doped ZnO Nanoparticles Obtained by Hydrothermal Synthesis. *Journal of Nanomaterials, 201*(86), 214-220.

Yang, X. (2008). Electrical and Optical Properties of Zinc Oxide for Scintillator Applications. Ph.D dissertation, Dept. App. Phys., West Verginia Univ., Morgantown, West Virginia.

Zegadi, C., Abderrahmane, A., Djelloul, A., Hamzaoui, S., Adnane, M., Chaumont, D., & Abdelkebir, K. (2015). Effects on structural and electro-optical properties of iron incorporation to p-zinc oxide (ZnO) thin films deposited by dip-coating process. *International Review of Physics, 9*(4), 39–45.

Zhang, Y., Ram, M.K., Stefanakos, E.K., & Goswami, D.Y. (2013). Enhanced photocatalytic activity of iron doped zinc oxide nanowires for water decontamination. *Surface & Coatings Technology*, *217*(61), 119–123.